1994ApJ...431..416P

THE ASTROPHYSICAL JOURNAL, 431:416–424, 1994 August 10
© 1994. The American Astronomical Society. All rights reserved. Printed in U.S.A.

THE CONTINUUM SPECTRAL CHARACTERISTICS OF GAMMA-RAY BURSTS OBSERVED BY BATSE

GEOFFREY N. PENDLETON, WILLIAM S. PACIESAS, MICHAEL S. BRIGGS,
ROBERT S. MALLOZZI, AND TOM M. KOSHUT
Department of Physics, University of Alabama in Huntsville, Huntsville, AL 35899

GERALD J. FISHMAN, CHARLES A. MEEGAN, ROBERT B. WILSON, AND ALAN B. HARMON
NASA/Marshall Space Flight Center, Huntsville, AL 35812

AND

CHRYSSA KOUVELIOTOU[1]
Universities Space Research Association
Received 1993 August 30; accepted 1994 February 10

ABSTRACT

Distributions of the continuum spectral characteristics of 260 bursts in the first BATSE catalog are presented. The data are derived from flux ratios calculated from the BATSE Large Area Detector (LAD) four-channel discriminator data. The data are converted from counts to photons using a direct spectral inversion technique to remove the effects of atmospheric scattering and the energy dependence of the detector angular response. Although there are intriguing clusterings of bursts in the spectral hardness ratio distributions, no evidence for the presence of distinct burst classes based on spectral hardness ratios alone is found. All subsets of bursts selected for their spectral characteristics in this analysis exhibit spatial distributions consistent with isotropy. The spectral diversity of the burst population appears to be caused largely by the highly variable nature of the burst production mechanisms themselves.

Subject heading: gamma rays: bursts

1. INTRODUCTION

This analysis of BATSE data (Fishman et al. 1989a, b) presents the coarse spectral characteristics of an ensemble of 260 gamma-ray bursts (GRBs) observed by BATSE from 1991 April 23 to 1992 March 5. Previous observations of GRBs (e.g., Higdon et al. 1990) have shown that they exhibit extremely hard spectra that are in general softer at higher energies than they are at lower energies (Wheaton et al. 1973; Cline et al. 1973). They can be characterized in general by a quasi-exponential component at lower energies and in some cases a power-law component at higher energies. Many bursts appear to be consistent with power-law spectra to 100 MeV (Matz et al. 1985; Kwok et al. 1993). Evidence for striking spectral diversity is present in the earlier measurements (Mazets et al. 1981) as well as in more recent analyses (Band et al. 1993). The data presented here are in agreement with the previously observed spectral behavior and provide an overview of the entire range of continuum spectra that bursts exhibit in the energy range from 25 to 2000 keV. The LAD data of unprecedented sensitivity are available for all the bursts in the viewing period specified above and provide one of the largest samples of burst spectral data from a single instrument to date.

2. ANALYSIS

The analysis primarily employed DISCSC (Summed LAD discriminator counts) and PREB (preburst) (Fishman et al. 1989) data for the bursts. The DISCSC data consist of four broad channels corresponding to the energy ranges 20–50 keV, 50–100 keV, 100–300 keV, and $E > 300$ keV for the BATSE LAD's. The data are summed over all detectors that measured the burst flux at a rate greater than or equal to 5.5 σ above background in the energy range 50–300 keV at the time of the burst trigger (Meegan 1991). They have 64 ms time resolution covering the time interval from the burst trigger to 240 s after the burst trigger. The PREB data have the same energy binning and time resolution as the DISCSC data. They are collected for each individual LAD in a sliding buffer that covers the interval from -2.0 s to the burst trigger time. For the purposes of this analysis the PREB data are summed over the detectors included in the DISCSC data. DISCLA (LAD discriminator) data with 1.024 s resolution were used for calculating background. If a burst had emission outside the -2 to 240 s interval covered by the combined PREB and DISCSC data, then background-subtracted DISCLA data were added to complete the fluence calculation.

Background subtraction was performed using a quadratic fit to the count rates in each channel of each detector derived from appropriate 1.024 s resolution background intervals around the burst. Figure 1 shows all the elements employed in the background subtraction for trigger 160 (1B 910507) in each discriminator channel. The reduced χ^2's for the background fit averaged ~ 1.13.

Two spectra were selected for each burst in this analysis: a 64 ms peak rate spectrum and a total fluence spectrum. The 64 ms peak spectrum was selected by choosing the interval with the largest count rate in discriminator channels 2 and 3 (50–300 keV) from the 64 ms data. The total fluence spectrum was produced by summing all the flux in the burst interval.

The counts data were converted to photons by applying two iterations of a direct matrix inversion technique. For this procedure detector response matrices (DRMs) (Pendleton et al. 1989) that included atmospheric scattering corrections (Pendleton et al. 1992) were generated for each burst. They

[1] Postal address: NASA/Marshall Space Flight Center, Huntsville, AL 35812.

© American Astronomical Society • Provided by the NASA Astrophysics Data System

1994ApJ...431..416P

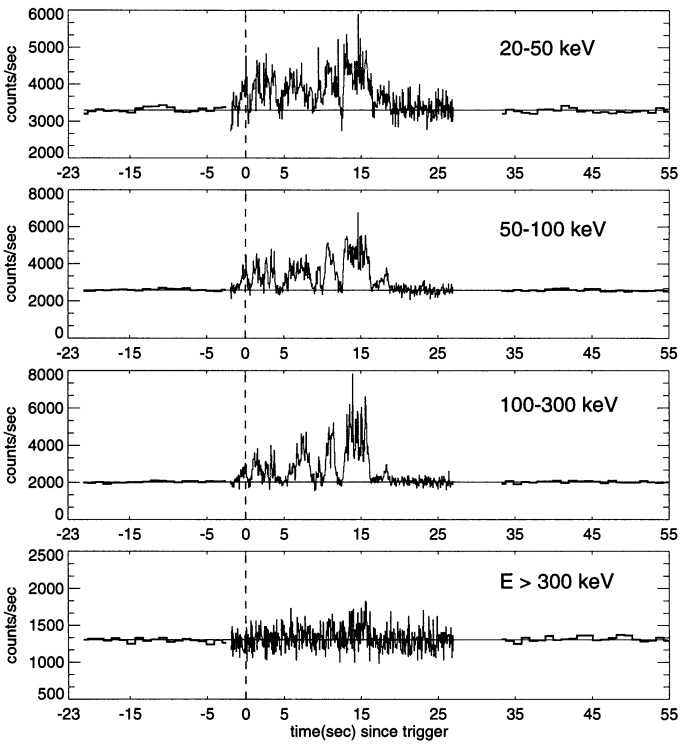

FIG. 1.—Histograms showing the source and background counts for channel 1: 20–50 keV, channel 2: 50–100 keV, channel 3: 100–300 keV, and channel 4: $E > 300$ keV for trigger 160 (1B 910507). The thin histogram at the center of each plot shows the source plus background data in each channel summed over detectors 1 and 3 on a 64 ms timescale. The thick histograms on either side show the 1.024 s time resolution data used for the quadratic background fit. The thin line spanning the entire interval shown is the quadratic background that is subtracted form the counts in the burst interval. The vertical dashed lines in the plots show the burst trigger time.

were binned with the four-channel energy resolution of the counts data. This broad energy binning of the DRM's necessitated the inclusion of some estimate of the spectral index of the incident photon spectrum across each bin. For example, 50 keV photons contribute to the four channel count spectra very differently from 100 keV photons. Having some estimate of the ratio of 50 to 100 keV photons in the incident spectra is important in order to convert the counts data to photon spectra accurately.

In the first iteration the matrices were generated with an assumed power-law index of -0.5 across the first three discriminator bins and an index of -1.1 in the $E > 300$ keV bin. Then, for each burst, the DRM was mathematically inverted. This inverted matrix then represented the quantitative conversion of observed counts to incident photons. The matrix multiplication of the four-element vector of counts data with the inverse DRM produced a four-element vector of photon data. The results of this first application of the matrix inversion procedure to the ensemble of burst data produced a wide variety of burst spectra. Many of these spectra had spectral indices that differed significantly from those applied across the matrix bins in the first iteration of the DRM calculations.

Assuming a spectral index across the matrix bin that more accurately represents the continuum spectrum being studied increases the accuracy of the spectral inversion technique. To obtain a first-order estimate of the spectral indices for the burst continuum spectra, a quadratic was fitted to the four-photon data points expressed in log (photons cm^{-2} keV^{-1}) versus the logarithmic bin centers expressed in log (keV). This is quantitatively equivalent to finding the best-fit parabola to the data on a log-log plot. This fit provides a first-order estimate of the amplitude and spectral index of the continuum for each data point.

The DRMs were then recalculated, weighting the spectra across the photon input bins using the slopes found with the quadratic fit in order to more accurately represent each burst continuum spectrum. These matrices were then inverted and applied to the counts data. In some cases the resulting photon spectra differ significantly from those of the first iteration in channel four ($E > 300$ keV). The other photon data remained quite stable between iterations.

The data presented here are expressed in the form of effective power-law spectral indices calculated for each pair of adjacent bins in the photon spectrum. The formula relating the ratio of photons observed in bins i and $i + 1$ to an effective power-law index, α is

$$\frac{\int_{E_i}^{E_{i+1}} E^{\alpha}\, dE}{\int_{E_{i+1}}^{E_{i+2}} E^{\alpha}\, dE} = \frac{P_i}{P_{i+1}}, \quad (1)$$

where P_i is the photon flux observed in the ith channel and P_{i+1} is flux in the $i + 1$th channel.

This equation was evaluated numerically over a range of α's for the three ratios of adjacent channels. The 1 σ error ranges on the photon data ratios were transformed via this equation to 1 σ error ranges on the effective spectral indices.

This technique was applied to Crab flux obtained with BATSE occulation software (Harmon et al. 1992) using DISCLA data to determine its accuracy. This analysis revealed that the LAD discriminator overflow bin (channel 4, $E > 300$ keV) was effectively represented by a detector response matrix element that extends from 300 to 6500 keV. It must be remembered, however, that there is no spectral information in this energy range in the DISCLA data. The channel 4 data can be used to determine if the higher energy flux is consistent with a particular simple spectral form but more detailed information must be obtained from data types with higher energy resolution.

There were bursts out of the set of 260 that did not have measurable flux in all channels for either the peak rate or total fluence. In the cases where only upper limits were available no spectral index was calculated. All 260 bursts had measurable flux in channels 2 and 3 as a consequence of the trigger criterion. However, some bursts did not have measurable flux in channels 1 and 4. Table 1 presents the totals of the bursts based on the significance of the observed rates in channels 1 and 4. The numbers in the channel 1 columns apply to bursts that have measurable flux in channel 1. Conversely, the No. Channel 1 columns refer to bursts without significant channel 1 flux. The rows are defined similarly for channel 4 flux. The totals are presented separately for the peak fluxes and total fluences.

3. PEAK FLUX AND FLUENCE SPECTRAL DISTRIBUTIONS

Effective power-law indices characterizing the peak flux and fluence continuum spectra of the bursts are presented as scatter plots and as histograms in Figures 2–9. Some numerical information is presented in tabular form. Figures 2*a*–4*d* show scatter plots of the spectral indices for the entire ensemble of bursts. These spectral indices are plotted with the higher

© American Astronomical Society • Provided by the NASA Astrophysics Data System

1994ApJ...431..416P

TABLE 1

TOTALS OF CHANNEL 1 AND 4 FLUX AND FLUENCE CASES

A. FLUX CASE			B. FLUENCE CASE		
Peak Flux	Channel 1	No Channel 1	Fluence	Channel 1	No Channel 1
Channel 4.....	169	23	Channel 4.....	209	4
No Channel 4.....	56	12	No Channel 4.....	47	0

energy indices on the vertical axis and the lower energy indices on the horizontal axis. Plotting these indices simultaneously gives an estimate of the curvature of the spectra over the total energy range displayed in the scatter plot. Also shown on these plots is a dotted line representing power-law spectra. Points below this line correspond to spectra that have a concave downward curvature on log-log plots of photons/kev versus photon energy. These are spectra that are softer at higher energies. Points above the power-law line correspond to spectra that are concave up on log-log plots (i.e., spectra that are harder at higher energies).

The upper left-hand plots (2*a*, 3*a*, and 4*a*) of these figures show the spectral indices of the 64 ms peak fluxes for the bursts. The spectral index axis limits for these plots were picked to focus on the distribution of the vast majority of bursts. (The histogram plots have larger ranges to show the extremes of the spectral index distributions.) Each square on these plots represents an individual burst. The error bars are omitted from these plots for clarity.

The effective spectral indices for Crab occultation data summed over 1 day for each of the 8 LAD detectors are shown as diamonds on these plots. The size of the diamonds show the errors for each point. These spectral indices are in reasonable agreement with previous measurements (Jung et al. 1989) of the steady Crab flux in the same energy range. Comparisons have been made between the burst spectral indices presented here and those obtained using the spectroscopy detector data (Band et al. 1993). There is agreement between the LAD and SPEC detector results when similar time and energy intervals are compared. In particular, Band's high-energy spectral indices

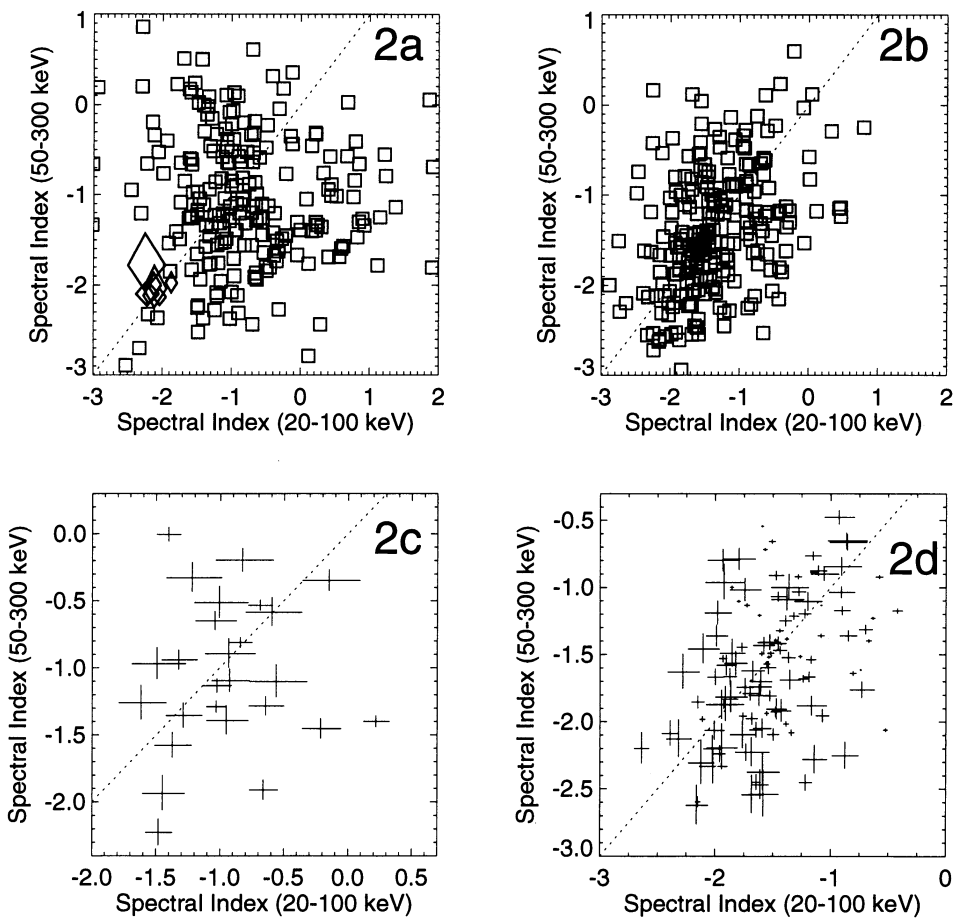

FIG. 2.—(*a–d*) These figures show scatter plots of power spectral indices for the 20–100 keV range vs. the 50–300 keV range for the gamma-ray bursts. The direct crab flux spectral indices are represented by diamonds on these plots. (*a*) 64 ms peak rate data. (*b*) Spectral indices of the total fluence. (*c*) Subset of the 64 ms peak flux data points where the errors in the spectral indices are less than 0.5 in both the 20–100 keV and 50–300 keV range. (*d*) Subset of the total fluence spectral indices with the same error constraints as (*c*).

© American Astronomical Society • Provided by the NASA Astrophysics Data System

1994ApJ...431..416P

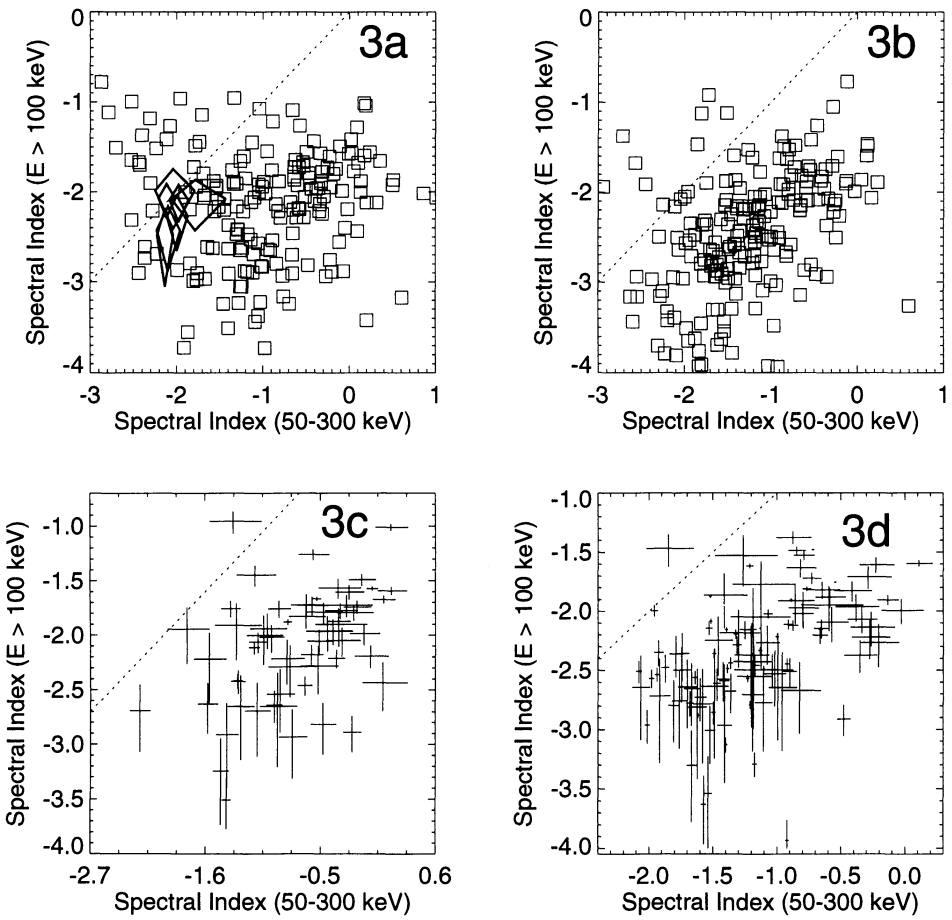

FIG. 3.—(*a–d*) The data in these figures are presented in the same format as in Fig. 2*a*–2*d* except that here the indices in the 50–300 keV range are compared to the indices for the energy $E > 100$ keV. The error constraints for (*c*) and (*d*) are data points with indices less than 0.5 in the 50–300 keV range and 1.0 in the $E > 100$ keV range.

for burst fluence measurements agree with those presented here for bursts 1B 910421, 1B 910629, and 1B 911118.

The lower left-hand plots (Figs. 2*c*, 3*c*, and 4*c*) are the subset of the data shown in the upper right-hand plots that are well determined and reveal some of the underlying structure of the spectral index distribution.

The right-hand plots mimic the left-hand plots in format. They show the spectral indices for the total fluence of the bursts. The integration times for these spectra range from 64 ms to hundreds of seconds. The longer integration times result in smaller errors as can be seen in the lower right-hand plots (Figs. 2*d*, 3*d*, and 4*d*).

The broad distribution of burst spectral states is evident in this data. One interesting feature of some of the 20–300 keV spectra shown in Figure 2 scatter plots is that they exhibit hardening of the spectra with energy up to 300 keV. Figure 2*d* shows burst fluences that are many sigma above the power-law line indicating concave up spectra. Spectra like these have been observed before (Mazets et al. 1981; Murakami et al. 1988). These kind of spectra may indicate the presence of more than one spectral component contributing to the spectra simultaneously. No significant evidence for this type of spectral behavior is evident in any of the other energy ranges studied here.

The higher energy range data shown in the Figure 3 plots show general concave down behavior above 50 keV. There is quite a range of spectral indices but the power-law line seems to be an upper bound for these spectra. In fact, most of the bursts show at least a 0.5 spectral index softening between the 50–300 keV range and the $E > 100$ keV range.

The total energy range ($E > 20$ keV) plots of Figure 4 also show spectra that in general become softer with increasing energy. In both the high-energy and total energy range plots there are bursts consistent with power-law spectra. However the plots showing spectra with smaller error bars show no significant number of bursts exhibiting concave up behavior over these energy ranges.

The spectral diversity of the burst population prompts the question of whether two or more subclasses of bursts can be resolved by studying the distribution of their spectral continuum properties. In fact, the original impetus for this research was to identify spectrally distinct subclasses of bursts that exhibited significantly different spatial distributions. For example, if a set of galactic disk objects observed well out into the disk were contributing bursts of one spectral type and cosmological sources were contributing bursts of another spectral type, then the spatial distributions of these two types of bursts would be different. No evidence for this type of behavior is seen in these data.

The scatter plots of the burst spectral characteristics show a complex distribution of GRB spectra that might possibly be

© American Astronomical Society • Provided by the NASA Astrophysics Data System

1994ApJ...431..416P

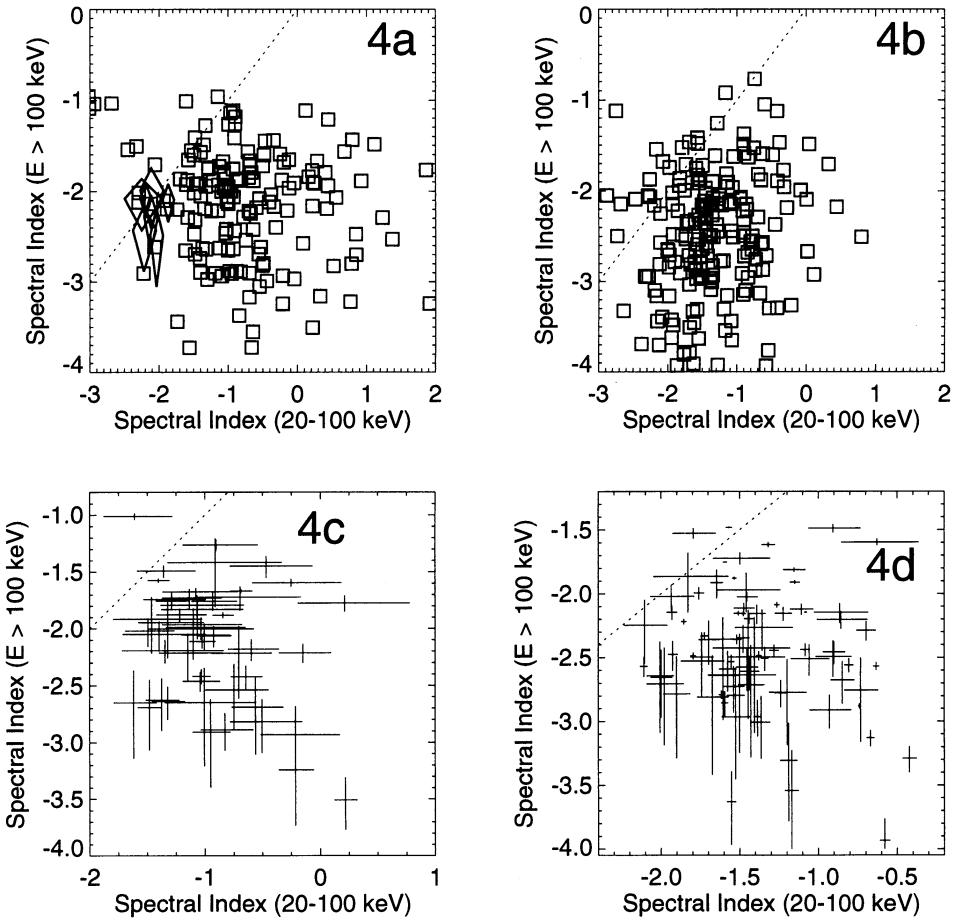

FIG. 4.—(*a–d*) The data here are presented in the same format as in Fig. 2*a–2d* except that here the indices in the 20–100 keV range are compared to the indices for the energy range $E > 100$ keV. The error constraints for (*c*) and (*d*) are data points with indices less than 0.5 in the 20–100 keV range and 1.0 in the $E > 100$ keV range.

resolved into a significantly multimodal distribution at some future time when enough bursts have been measured. Already a bimodal duration distribution has been identified in the BATSE burst data (Kouveliotou et al. 1993). The bursts in the short duration class show significantly harder fluences on average than the longer duration bursts. Figure 5 shows the spectral index of the total fluence in the 50–300 keV range versus burst duration. This plot is quite similar to Figure 4 of Kouveliotou et al. (1993). The Spearman rank-order analysis shows a correlation between hardness and duration with a chance fluctuation probability of 2×10^{-7}. However the range of spectral behaviors exhibited by both the short- and long-duration bursts is quite broad, and they cannot be confidently isolated from each other using the data set presented here. This conclusion is also reached by Kouveliotou et al. (1993).

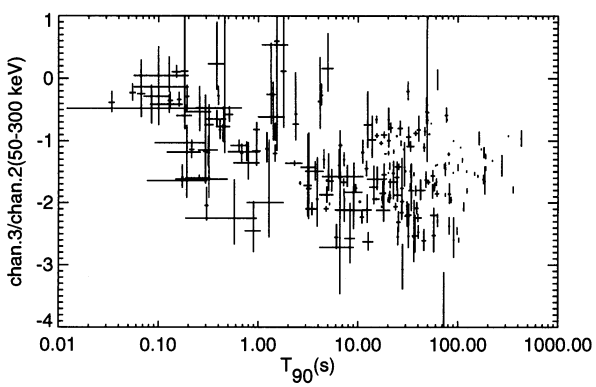

FIG. 5.—The spectral indices of the bursts total fluences in the energy range 50–300 keV are plotted vs. duration (T_{90}). Here T_{90} is defined (see Kouveliotou et al. 1993) as the length of the interval containing the middle 90% of the burst fluence.

Spatial distributions of possible spectral subsets of bursts were studied and found to be consistent with isotropy. Figures 2*b* and 2*d* show some clustering of burst fluences about a spectral index of approximately -1.7 in the 50–300 keV and 20–100 keV ranges. There are some other bursts loosely scattered around -1.0 on these plots as well. The bursts were split into two sets centered about these spectral indices; however the spatial distributions of these two sets are consistent with isotropy. Table 2 shows dipole $\langle \cos \theta \rangle$ and quadrapole $\langle \sin^2 b - \frac{1}{3} \rangle$ moments calculated in galactic coordinates of spectral subsets of bursts. Also shown in the table are the values expected for a uniform distribution viewed through the BATSE sky map. The inequalities in the table show the dividing lines between the spectral subsets. There are also bursts which show a dearth of emission above 300 keV. These bursts, without significant flux/fluence in channel 4 (see Table 1), are consistent with isotropy as well.

© American Astronomical Society • Provided by the NASA Astrophysics Data System

1994ApJ...431..416P

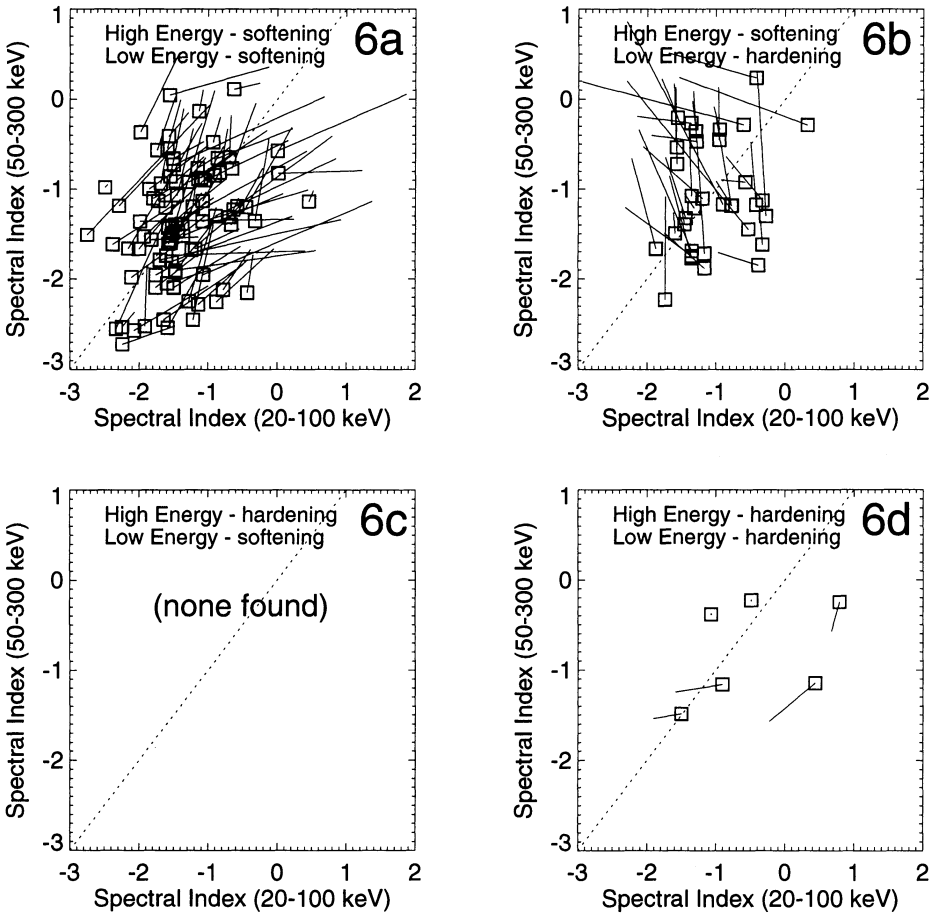

FIG. 6.—(*a–d*) These figures show scatter plots of the changes in spectral power indices between the 64 ms peak fluxes and the total fluences for the 20–100 keV range vs. the 50–300 keV ranges. The squares in these plots are the total fluence points. The lines extending from these boxes end at the 64 ms peak spectra points. These lines show the direction of the spectral changes between peak flux and total fluence of the power-law indices for the bursts. The data are separated into four plots to aid in visual interpretation. The upper left-hand plot shows softening of both the higher energy and lower energy total fluence spectral indices with respect to the peak flux indices. The upper right hand plot shows softening of the higher energy indices and hardening of the lower energy indices. The lower left-hand plot shows hardening of the higher energy indices and softening of the lower energy indices. The lower right-hand plot shows hardening of both the higher energy indices and the lower energy indices.

4. CHANGES OF SPECTRAL INDICES WITHIN BURSTS

There is significant variability of the spectra within individual bursts. The changes in spectral indices for bursts between their 64 ms peak spectra and the total fluence spectra are shown in the scatter plots of Figures 6*a*–8*d*.

The spectral changes shown in the Figure 6 plots show mostly a softening of the fluence relative to the peak spectrum in the 20–100 keV range. This softening trend occurs in an even larger fraction of the bursts in the 50–300 keV range. It is interesting to note that none of the bursts showed a hardening of the fluence with respect to the peak spectrum in the 50–300 keV range coupled with a softening in the 20–100 keV range.

These spectral index change plots show in general a tendency toward softening of the fluence spectra with respect to the peak spectra. Only a few events exhibit hardening of the

TABLE 2

SPATIAL MOMENTS OF SPECTRAL SUBSETS

Subset Constraints Uniform Distribution	$\langle\cos\theta\rangle$ of Subset -0.013	$\langle\sin^2 b - \frac{1}{3}\rangle$ of Subset -0.005
$IF^{a}_{32} > -0.71IF_{21} - 2.26$	0.016 ± 0.047	-0.037 ± 0.024
$IF_{32} < -0.71IF_{21} - 2.26$	0.017 ± 0.055	-0.016 ± 0.029
$IP^{b}_{32} > -0.27IP_{21} - 1.01$	0.052 ± 0.055	-0.038 ± 0.028
$IP_{32} < -0.27IP_{21} - 1.01$	-0.010 ± 0.047	-0.020 ± 0.025
No channel 4 peak flux	-0.001 ± 0.070	0.021 ± 0.036
No channel 4 fluence	-0.008 ± 0.068	-0.015 ± 0.035

[a] IF_{32} is the fluence spectral index across channels 2 and 3.
[b] IP_{32} is the peak flux spectral index across channels 2 and 3.

© American Astronomical Society • Provided by the NASA Astrophysics Data System

1994ApJ...431..416P

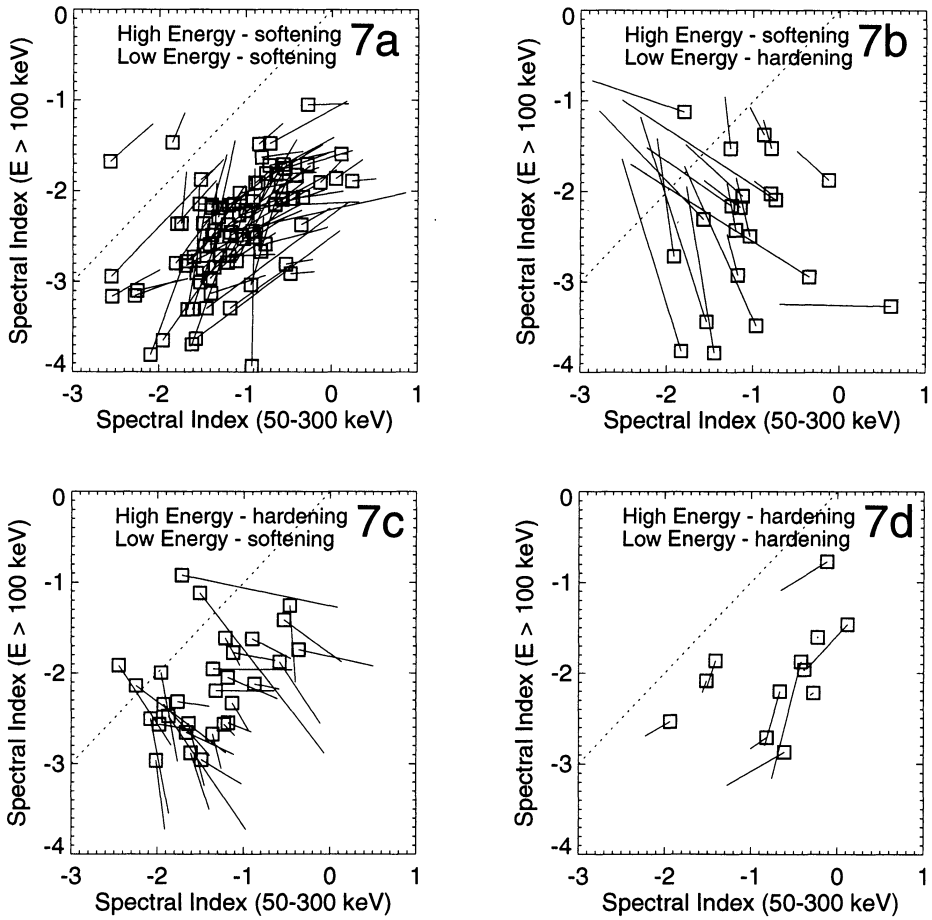

FIG. 7.—(*a–d*) These plots have the same format as plots Figs. 5*a–5d*. Here the changes in spectral indices between peak flux and total fluence are being shown for the 50–300 keV range and the $E > 300$ keV range.

fluence spectra with respect to the peak spectra (Fig. 6*d*, 7*d*, and 8*d*).

Figures 9*a–9c* compare the peak flux and fluence spectral index distributions in histogram form. Quantitative studies of these spectral index distributions have been made on appropriate sets of bursts. For each energy range bursts were selected that had measurable spectral indices in both the peak spectra and fluence spectra. Table 3 summarizes the averages of the spectral index distributions. Here column (2) shows the number of bursts in each set. Column (3) contains the average of the fluence spectra distribution in the specified energy range. Column (4) contains the same information for the 64 ms peak spectra. Column (5) contains the average of the peak spectra distribution corrected for selection effects.

There are two selection effects that impact the peak rate spectra due to the fact that there are on average ~10 64 ms spectra within 1 σ of the peak spectrum in the 50–300 keV range. One effect is that selecting the brightest of these spectra based on the 50–300 keV counts flux will generally result in the highest statistical fluctuations being chosen for channels 2 and 3. Since channels 1 and 4 are outside this energy range, they will not be subject to the same statistical selection effect and only values distributed about the average intensity near the peak will be chosen. However, countering this effect is the detector response characteristic that a continuum of photons spanning channel 1 will produce some counts in channel 2 as well due to the width of the detector resolution. High-energy photons that mainly contribute to channel 4 sometimes are recorded in the lower channels instead due to partial energy deposition. Hence higher rates in channels 1 and 4 imply some spill over to channels 2 and 3. Monte Carlo simulations were made to quantify the impact of these selection effects on the peak rate spectral index calculations as a function of intensity, spectral index, and number of 64 ms spectra within 1 σ sigma of the peak. The results of the simulations were applied to the observed data to produce the corrected averages.

The general softening of the fluence with respect to the peak flux is evident in the Figure 9 plots and the Table 3 data, particularly in the 20–100 keV range. These results mean that the more intense portions of bursts are usually comprised of harder spectra than the less intense portions, but this does not necessarily apply to all bursts. It is also clear that the spectra

TABLE 3

SPECTRAL INDEX DISTRIBUTION AVERAGES

Energy Range (keV) (1)	Number of Bursts (2)	Fluence Average (3)	Peak Average (4)	Corrected Peak Average (5)
20–100	224	-1.41 ± 0.050	-0.73 ± 0.075	-0.71
50–300.....	260	-1.38 ± 0.055	-1.13 ± 0.057	-1.09
$E > 100$	164	-2.46 ± 0.069	-2.19 ± 0.058	-1.96

© American Astronomical Society • Provided by the NASA Astrophysics Data System

1994ApJ...431..416P

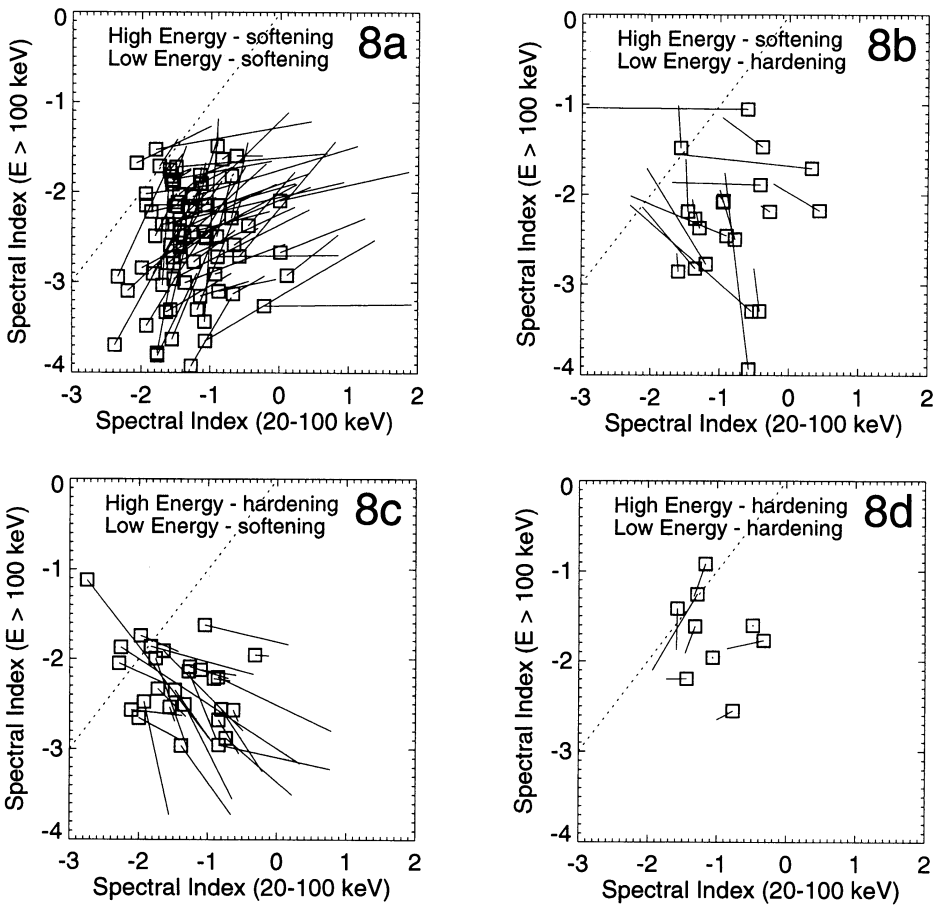

FIG. 8.—(*a–d*) These plots have the same format as plots in Figs. 5*a–5d* plots. Here the changes in spectral indices between peak flux and total fluence are being shown for the 20–100 keV range and the $E > 300$ keV range.

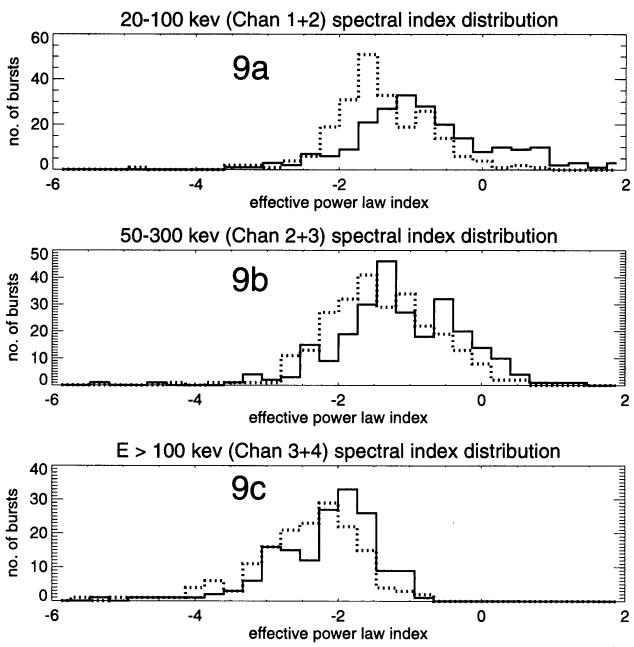

FIG. 9.—(*a–d*) These are histograms of the spectral indices over the three energy ranges studied here. The solid lines represent the distribution for the peak rate spectra and the dotted lines show the distribution for the total fluence spectra. (a) The spectral index distributions for the energy range 20–100 keV, (*b*) 50–300 keV, (*c*) $E > 100$ keV.

change significantly within individual bursts. These results are consistent with previous burst studies. A point that can be emphasized with this large and exhaustive burst data set is that the spectral changes between peak flux and fluence for individual bursts can span a significant portion of the spectral range of the entire burst distribution. This behavior suggests that the highly variable nature of the burst emission mechanisms may be responsible for the variety of burst spectra observed. It is likely that the bursts observed share common physical production mechanisms that happen to be highly variable.

Another qualitative observation of the 20–100 keV histograms is that the distribution of average spectral indices appears to have more clustering in it than the peak spectral index distribution. However, the distribution widths are dependent on the statistical significance of the two data sets. Simulations show that the difference in the width of the peak flux and fluence distributions is consistent with the differences in the statistical significances of these data sets.

5. SUMMARY

In general, the burst spectra are softer at higher energies than at lower energies. This is consistent with other observations (Mazets et al. 1981). Some of the spectra seem to have complex spectral structure switching from concave down to concave up over different energy ranges. Complex spectral structure has been noted in bursts before as well (Mazets et al. 1988; Mitrofanov et al. 1992). There is no evidence for clearly

© American Astronomical Society • Provided by the NASA Astrophysics Data System

1994ApJ...431..416P

independent spectral classes of objects manifesting their existence through this analysis. The spatial distributions of all subsets examined are consistent with the entire burst ensemble distribution. It seems more likely that the spectral diversity of the burst phenomenon represents the variable nature of the physical mechanisms that produce the bursts rather than the superposition of sets of unrelated astrophysical objects with distinct, less variable spectra.

Variability of the burst production mechanisms is evident in the spectral changes observed within individual bursts. Comparisons of the peak flux spectra to the total fluence spectra show that in general the peak flux is significantly harder than the total fluence in the energy range 20–100 keV. The peak flux is harder than the total fluence in the 50–300 keV and the $E > 300$ keV ranges as well, although the effect is not as significant.

REFERENCES

Band, D. L., et al. 1993, ApJ, 413, 281
Cline, T. L., Desai, U. D., Klebesadel, R. W., Strong, I. B., et al. 1973, ApJ, 185, L1
Fishman, G. J., et al. 1989a, in Proc. GRO Science Workshop, Vol. 2, ed. N. Johnson (Washington, DC: NRL), 39
———. 1989b, in Proc. GRO Science Workshop, Vol. 3, ed. N. Johnson (Washington, DC: NRL), 47
Harmon, B. A., et al. 1993 in Proc. Compton Observatory Science Workshop, ed. R. Shrader, N. Gehrels, & B. Dennis (NASA CP 3137), 69
Higdon, J. C., & Lingenfelter, R. E. 1990, ARA&A, 28, 401
Jung, G. V. 1989, ApJ, 338, 972
Kouveliotou, C., Meegan, C. A., Fishman, G. J., Bhat, N. P., Briggs, M. S., Koshut, T. M., Paciesas, W. S., & Pendleton, G. N. 1993, ApJ, 413, L101
Kwok, P. W., et al. 1993, in AIP Conf. Proc. 280, Proc. Compton Gamma-Ray Observatory Conf., ed. M. Friedlander, N. Gehrels, & D. Macomb (New York: AIP), 885
Matz, S. M., et al. 1985, ApJ, 288, L37
Mazets, E. P., et al. 1981, Ap&SS, 80, No. 1, 3
———. 1988, Adv. Space Res., Vol. 8, No. 2–3, (2) 669
Meegan, C. A. 1991, in BATSE Flight Software User's Manual
Mitrofanov, I. G., et al. 1992, in Gamma-Ray Bursts: Observations, Analyses, and Theories, ed. C. Ho, R. Epstein, & E. Fenimore (Cambridge Univ. Press), 209
Murakami, T., et al. 1988 Nature, 335, 234
Pendleton, G. N., Paciesas, W. S., Lestrade, J. P., Fishman, G. J., Wilson, R. B., & Meegan, C. A. 1989, in Proc. GRO Science Workshop, Vol. 4, ed. N. Johnson (Washington, DC: NRL), 547
Pendleton, G. N., et al. 1992, in Proc. Compton Observatory Science Workshop, ed. R. Shrader, N. Gehrels, & B. Dennis (NASA CP 3137), 47
Wheaton, W. A., et al. 1973, ApJ, 185, L57

© American Astronomical Society • Provided by the NASA Astrophysics Data System